Sources of CO_2 Produced in Freshly Thawed Pleistocene-Age Yedoma Permafrost

Jan Olaf Melchert[1], Philipp Wischhöfer[1], Christian Knoblauch[2,3], Tim Eckhardt[2,3], Susanne Liebner[4,5] and Janet Rethemeyer[1]*

[1]Institute for Geology and Mineralogy, University of Cologne, Cologne, Germany, [2]Institute for Soil Science, Universität Hamburg, Hamburg, Germany, [3]Center for Earth System Research and Sustainability, Universität Hamburg, Hamburg, Germany, [4]German Research Centre for Geosciences (GFZ), Helmholtz Centre Potsdam, Potsdam, Germany, [5]Institute of Biochemistry and Biology, University of Potsdam, Potsdam, Germany

The release of greenhouse gases from the large organic carbon stock in permafrost deposits in the circumarctic regions may accelerate global warming upon thaw. The extent of this positive climate feedback is thought to be largely controlled by the microbial degradability of the organic matter preserved in these sediments. In addition, weathering and oxidation processes may release inorganic carbon preserved in permafrost sediments as CO_2, which is generally not accounted for. We used ^{13}C and ^{14}C analysis and isotopic mass balances to differentiate and quantify organic and inorganic carbon released as CO_2 in the field from an active retrogressive thaw slump of Pleistocene-age Yedoma and during a 1.5-years incubation experiment. The results reveal that the dominant source of the CO_2 released from freshly thawed Yedoma exposed as thaw mound is Pleistocene-age organic matter (48–80%) and to a lesser extent modern organic substrate (3–34%). A significant portion of the CO_2 originated from inorganic carbon in the Yedoma (17–26%). The mixing of young, active layer material with Yedoma at a site on the slump floor led to the preferential mineralization of this young organic carbon source. Admixtures of younger organic substrates in the Yedoma thaw mound were small and thus rapidly consumed as shown by lower contributions to the CO_2 produced during few weeks of aerobic incubation at 4°C corresponding to approximately one thaw season. Future CO_2 fluxes from the freshly thawed Yedoma will contain higher proportions of ancient inorganic (22%) and organic carbon (61–78%) as suggested by the results at the end, after 1.5 years of incubation. The increasing contribution of inorganic carbon during the incubation is favored by the accumulation of organic acids from microbial organic matter degradation resulting in lower pH values and, in consequence, in inorganic carbon dissolution. Because part of the inorganic carbon pool is assumed to be of pedogenic origin, these emissions would ultimately not alter carbon budgets. The results of this study highlight the preferential degradation of younger organic substrates in freshly thawed Yedoma, if available, and a substantial release of CO_2 from inorganic sources.

Keywords: yedoma ice complex, permafost, carbon cycle, climat change, thermokarst, radiocarbon, greenhouse gas

INTRODUCTION

Permafrost deposits in the northern circumpolar regions contain about 1,300 to 1,600 Gt of organic carbon (OC) that accumulated over thousands of years and was stored at sub-zero temperatures (Schuur et al., 2015). More than one quarter, about 327–466 Gt OC, is stored in the loess-like Yedoma sediments that were deposited during the late Pleistocene and early Holocene in unglaciated areas of the Arctic region (Schirrmeister, 2011; Strauss et al., 2017). These up to 50 m thick sediments include massive syngenetic ice wedges (Schirrmeister, 2011) resulting in very high ground ice contents of up to 80 vol.% (Strauss et al., 2017), thus making Yedoma deposits especially vulnerable to rapid thaw in a warming world. The melting of the ground ice due to rising ground temperatures (Biskaborn et al., 2019) causes surface subsidence and thereby may expose the sedimentary OC abruptly to microbial degradation (Czudek and Demek, 1970; Grosse et al., 2011; Strauss et al., 2017; Nitzbon et al., 2020; Turetsky et al., 2020). In consequence, the previously freeze-locked organic matter (OM) is decomposed and released to the atmosphere as carbon dioxide (CO$_2$), methane (CH$_4$), and other greenhouse gasses (GHGs) causing a positive climate feedback (Schuur et al., 2015).

The extent of the permafrost-carbon feedback is still under debate because it not only depends on OC quantity but also on OM quality, i.e., microbial degradability, which is still uncertain due to the limited analytical data. Most studies assessing OM quality and degradability, respectively rely on incubation experiments at different temperatures (Schädel et al., 2014, Schädel et al., 2016). The results of these laboratory studies may not necessarily apply to natural, more complex conditions. Additionally, chemical characterizations of the OM have been used to differentiate potentially labile and more recalcitrant OC pools based on OC/N ratios (e.g., Schädel et al., 2014; Kuhry et al., 2020) and characteristic organic compounds used as indicators for OM bioavailability and stage of degradation, respectively (e.g., Routh et al., 2014; Strauss et al., 2015; Stapel et al., 2016; Tanski et al., 2017; Jongejans et al., 2021).

Yedoma deposits were assumed to contain OM that accumulated and was freeze-locked quickly and thus has not undergone intense decomposition processes. Less transformed OM is supposed to be more reactive and thus more easily degradable upon thaw, which was reflected by high CO$_2$ fluxes measured in some incubation studies (Dutta et al., 2006; Zimov et al., 2006; Knoblauch et al., 2013) and the presence of easily biodegradable substrates (Stapel et al., 2016; Jongejans et al., 2018). In contrast, other studies measured a higher degree of OM decomposition (Kuhry et al., 2020), which, however, did not result in lower respiration rates during some incubation studies (Weiss et al., 2016). The contrasting results may be attributed to the large spatial and temporal variability of OC contents and OM composition in Yedoma deposited under different environmental and climatic conditions (Strauss et al., 2015; Weiss et al., 2016; Stapel et al., 2018; Walz et al., 2018; Windirsch et al., 2020). In addition, thermokarst may alter the degradability of the ancient Yedoma OM by introducing younger material from overlying

TABLE 1 | Sampling locations on Kurugnakh Island and thaw depth (measured in August 2017).

Site		North [°DEC]	East [°DEC]	Thaw depth [cm]
TM2	Thaw mound	72.33920	126.29199	70
SF3	Thaw slump floor	72.33900	126.29207	78
HT1	Holocene terrace	72.33914	126.28945	21

sediments and changing thermal and hydrological conditions (Grosse et al., 2011; Strauss et al., 2015; Wild et al., 2016). The mixing of sediments is particularly pronounced on retrogressive thaw slumps, a dynamic form of thermokarst in ice-rich areas, expanding inland by melting of the ground ice in the headwall (Lantuit and Pollard, 2008; Costard et al., 2021).

The release of GHGs deriving from the mineralization of modern and ancient OM can be differentiated by ^{14}C analyses, which has been applied in several field and incubation studies in high latitude regions (e.g., Schuur and Trumbore, 2006; Czimczik and Welker, 2010; Estop-Aragonés et al., 2018). In addition, organic and inorganic carbon sources can be identified and quantified by their δ^{13}C signature and by applying a dual isotopic mass balance calculation (Dorsett et al., 2011; Griffith et al., 2012; Pries et al., 2016). The contribution of inorganic carbon (IC) to CO$_2$ fluxes that may be released by abiotic processes (e.g., Biasi et al., 2008; Tamir et al., 2011; Ramnarine et al., 2012) has been neglected in most previous studies, which may thus have overestimated GHG fluxes from the mineralization of OC. Yedoma deposits contain substantial amounts of carbonates of about 0.2–18% in the north-east Siberian coastal lowlands (Schirrmeister, 2011) that may be released by dissolution processes (Zolkos et al., 2018, Zolkos et al., 2020).

The aim of this study is to quantify and differentiate between ancient and modern OC as well as IC contributions to the CO$_2$ emissions released from a retrogressive thaw slump in a Yedoma deposit in north-east Siberia by using a dual carbon isotopic approach. We selected two study sites on the thaw slump where freshly thawed Yedoma is 1) exposed as thaw mounds and 2) mixed with substrates from the overlaying Holocene terrace. To differentiate between Pleistocene and Holocene substrates, a third site on the Holocene terrace was sampled additionally. Beside field measurements, we incubated the sediments for 1.5 years and analyzed the isotopic compositions of the CO$_2$ after a few weeks and at the end of the long-term incubation. In addition, we analyzed the composition of the OM in the thaw layer at all sites to elucidate their potential effects on CO$_2$ production rates.

STUDY SITE

The retrogressive thaw slump is located on the island of Kurungnakh, which lies beside the Olenyeksky Channel, in the southern part of the Lena River Delta in north-eastern Siberia (**Table 1**). Kurungnakh Island is mainly composed of late Quaternary sediments, so-called Yedoma or Ice Complex (Schirrmeister, 2011), which are up to 40 m thick and contain
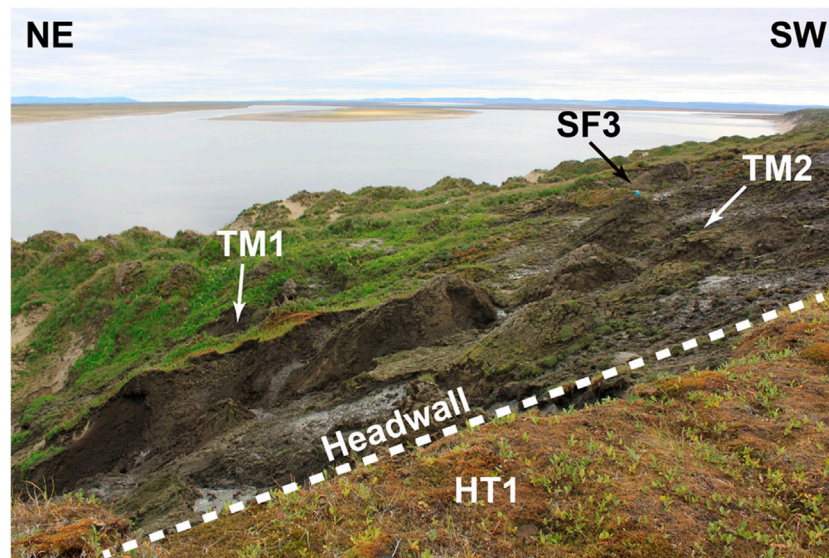
FIGURE 1 | Study sites on the retrogressive thaw slump on Kurungnakh Island including two thaw mounds (TM) in Pleistocene Yedoma, a site on the slump floor (SF) where sediments were mixed, and the Holocene terrace (HT).

large ice wedges resulting in ground-ice contents of up to 80 vol.% (Wetterich et al., 2008a; Schirrmeister, 2011). The Pleistocene-age Yedoma deposit is overlain by Holocene polygonal tundra (Grigoriev, 1993; Schwamborn et al., 2002). The surface layer of the Yedoma deposits thaws for about 4 months per year during summer (Boike et al., 2008) and may reach a depth of about 80 cm (**Table 1**). Recorded data for the years 1998–2011 document an annual mean air temperature of −12.5°C (measured on the nearby Samoylov Island), with maximum mean air temperatures of 10.1°C in July and 8.5°C in August (Boike et al., 2013). The mean annual precipitation (rainfall and snow water equivalent) is about 190 mm (Boike et al., 2013).

For this study, three different sites were selected on the retrogressive thaw slump about 15–35 m above river level including the overlying Holocene terrace (HT1), an intact thaw mound of Pleistocene Yedoma (TM2), and a site on the slump floor (SF3) where both types of sediments were mixed during erosion (**Figure 1**).

METHODS

Sediment Sampling

Samples were collected from the active layer of the soil in the Holocene terrace and the Yedoma sediment in August 2017. At each site, one soil pit of about 1 × 1 m was dug down to the to the frozen ground and four replicates were sampled from the pit wall using a hand shovel. Samples were collected in 10 cm intervals for bulk elemental analysis. The incubation experiment was conducted with replicates of up to four depth intervals per site. Therefore, some of the sampled depth intervals were combined and homogenized. All samples were stored in sealed plastic bags and kept frozen at −20°C until analysis.

Gas Sampling

Carbon dioxide was collected from three locations in about 0.5–1 m distance at each study site according to Wotte et al. (2017) using PVC collars that were placed on the sediment. At SF3 and TM2, sprouts were carefully removed from the mostly barren soil surface to prevent the contribution of autotrophic (plant) respiration. At HT1, aboveground vegetation was clipped with a knife and the uppermost 8 cm of the sediment were carefully removed from the ground to minimize contributions from autotrophic respiration.

The plastic collars (polyvinylchloride, 25 cm OD, 25 cm height) were placed 10 cm in the ground and left for 12 h prior to measurement. On the day of the measurement, an opaque chamber was placed on top of the collars and connected to an infrared gas analyzer (LI-840A, LI-COR Biosciences, Lincoln, United States). After closure of the chamber, the air was pumped in a closed loop for 5 min for CO_2 flux measurement. Moisture was removed using two traps filled with phosphorous pentoxide (Sicapent®, MERCK, Germany). Afterwards, atmospheric CO_2 was removed by pumping three chamber volumes through a soda lime trap (MERCK, Germany). Then, CO_2 emitted from the ground was trapped on a molecular sieve cartridge (MSC) filled with zeolite type 13X. The sampling time was about 30 min per site depending on CO_2 fluxes and volume of the emission chamber aiming to collect 2 mg of CO_2 on each MSC.

CO_2 fluxes were calculated from the recorded increase in CO_2 concentration inside the chamber during the first 5 minutes after closure. The first 30 s were discarded due to possible disturbances by closing the chamber. From the remaining data, the 2-min interval with the highest Pearson correlation coefficient (>0.9) was chosen for flux calculation.

Incubations

An aerobic long-term incubation experiment was conducted over a course of 1.5 years according to Knoblauch et al. (2013). Briefly, splits of the frozen sediment samples were thawed at 2°C and kept at 4°C for the duration of the incubation. The water content of each sample was determined prior to the start of the incubation. About 20 g of homogenized sediment was placed in 120 ml glass bottles, which were sealed by rubber stoppers and kept closed during the experiment to maintain constant moisture. The headspace of the bottles was flushed repeatedly with synthetic air prior to the start of the experiment to remove ambient CO_2 from each bottle. The CO_2 concentrations were recorded every week for the first 200 days and about every other month thereafter. If CO_2 concentrations exceeded 3%, the headspace was flushed repeatedly with synthetic air (20% O_2, 80% N_2). CO_2 samples were taken for isotope analysis at two times during the incubation: first, between 41 and 189 days after the samples had been flushed and again reached concentrations of about 3% CO_2. The second gas sampling was performed at the end of the experiment on day 537, regardless of the CO_2 concentration inside the bottles.

Sediment Analysis

Bulk sediment analysis was performed on freeze-dried samples that were ground and thereby homogenized using a porcelain mortar. Total carbon (C), total OC and total nitrogen (N) contents were quantified using an elemental analyzer (vario MICRO, Elementar, Germany). For OC analysis, aliquots of the sediment were decalcified by treatment with 40 ml of 1% hydrochloric acid (HCl) for 1 h at 60°C following 12 h at room temperature as described in Rethemeyer et al. (2019). After the acid treatment, the samples were washed to neutral pH by adding Mili-Q water and dried at 60°C. pH values were measured after DIN ISO 10390:2005-12 in a suspension of 5 g dry mineral soil and 25 ml Milli-Q water after shaking (1 h) and settling (1 h) using a pH meter (FE20, Mettler-Toledo, Ohio, United States).

Radiocarbon Analysis

[14]C analysis of the bulk OC was performed by combustion and graphitization of the CO_2 as described in Rethemeyer et al. (2019). In short, an aliquot of the decalcified sediment was weighed into solvent-cleaned tin boats (4 × 4 × 11 mm, Elementar, Germany) for subsequent combustion in an elemental analyzer (VarioMicroCube, Elementar, Germany). The CO_2 produced was converted to elemental carbon ("graphite") in an automated graphitization system (AGE; Wacker et al., 2010) using hydrogen and iron powder as catalyst. The ^{14}C content of the IC was measured by hydrolyzing the sediment, with phosphoric acid (99%) for 6 h at 75°C. This was done without prior removal of OC from the sediment. Although experiences with this method were positive, we cannot exclude that small amounts of OC were dissolved along the IC and contributed to the ^{14}C analysis. The CO_2 evolved was then transferred into the AGE system with He and converted to graphite. The graphite was pressed into AMS target holders, which were analyzed with the 6 MV accelerator mass spectrometer (AMS) at CologneAMS (Dewald et al., 2013).

The CO_2 trapped on the MSCs was processed on a vacuum rig as described in Wotte et al. (2017). The MSC was heated to 500°C to release the CO_2 from the zeolite and flushed with He (grade 4.6) via a water trap immersed in dry ice-ethanol mixture (−80°C) to a CO_2 trap placed in liquid nitrogen. The amount of CO_2 was quantified in a calibrated volume with a pressure sensor and the glass tube containing the CO_2 was flame sealed.

The CO_2 from the aerobic incubation experiment was recovered from the glass bottles using sterile hypodermic needles. Similar to the MSC desorption procedure, the incubation-derived CO_2 was purified, quantified and flame sealed on the vacuum rig. [14]C analysis of the CO_2 was performed using the gas ion source of the AMS at the University of Cologne and the gas injection system described in (Stolz et al., 2017). [14]C results are reported in $F^{14}C$ (Reimer et al., 2013) and as uncalibrated years before present (BP; Stuiver and Polach, 1977).

Stable Carbon Isotope Analysis

Stable carbon isotopes of OC were measured in sediment samples, which were decalcified with phosphoric acid, using an elemental analyzer (Flash 2000; Thermo Scientific, Germany) coupled to a Delta V (Thermo Scientific, Germany) isotope ratio mass spectrometer (IRMS) (Knoblauch et al., 2013). For $\delta^{13}C$ analysis of IC, ground sediment aliquots were weighed into 50 ml glass bottles and closed with a rubber stopper. Ambient air was removed from the bottles using He and phosphoric acid (5%) was added to convert the IC into CO_2. Carbon dioxide stable isotope analyses from IC, the incubation experiments and field samples were conducted by injecting gas samples into a Trace GC 1310 gas chromatograph connected to a DeltaVPlus IRMS (Thermo Scientific, Germany) (two replicates per sample). The range of replicate measurements was equal to or less than ±0.3‰. The results of the stable carbon isotope measurements were calibrated with external standards and are reported in permille relative to the Vienna Pee Dee Belemnite (‰ VPDB).

Statistics and Calculations

CO_2 production rates were compared with the elemental and isotopic compositions and the pH of the sediments using the ANOVA add-in from Microsoft Excel. For better comparison, the CO_2 production rate after 175 days of the incubation and at the end of the experiment, after 537 days, were used. Additionally, the CO_2 production rates were normalized for the amount of C available in the sample to eliminate bias by different C quantities. Furthermore, Pearson correlation coefficients were calculated to evaluate possible correlations between the data sets. Variances of data were compared using a F-test. Mean values of data sets were then compared using a t-test assuming either same or different variances, based on the F-test run previously.

The CO_2 samples taken from respiration chambers might contain contributions from atmospheric CO_2 leaking into the system through small cracks in the soil next to the chamber. To account for this effect, [14]C ($F^{14}C_s$) and [13]C ($\delta^{13}C_s$) contents of the CO_2 samples were corrected for the fraction of atmospheric CO_2 (f_{atm}) contributing to the total CO_2 and reported as $F^{14}C_c$. The $\delta^{13}C$ value of the CO_2 released in the incubation experiment

TABLE 2 | $\delta^{13}C$ and $F^{14}C$ values of the sedimentary C sources used in the mass balance calculation.

Site	$\Delta^{13}C$			$F^{14}C$		
	IC	OCa	OCy	IC	OCa	OCy
TM2	−5.26	−26.8	−27.8	0.044	0.042	0.984
SF3	−7.46	−25.6	−27.8	0.047	0.038	0.984
HT1	-	−29.4	−27.3	-	0.597	1.021

($\delta^{13}C_{inc}$) is free of atmospheric contamination that may be introduced in the field. It thus was used to correct the $\delta^{13}C$ values of the CO_2 sampled in the field ($\delta^{13}C_c$). In addition, the ^{14}C ($F^{14}C_{atm}$) and ^{13}C contents ($\delta^{13}C_{atm}$) of an atmospheric air sample taken from HT1 were used to calculate the fraction of atmospheric CO_2 (f_{atm}) in the CO_2 samples and correct their ^{14}C content ($F^{14}C_c$) according to **Eq. 1** and **Eq. 2**.

$$F^{14}C_c = \frac{(F^{14}C_s - f_{atm}*F^{14}C_{atm})}{(1 - f_{atm})} \quad (1)$$

with

$$f_{atm} = \frac{(\delta^{13}C_s - \delta^{13}C_{inc})}{(\delta^{13}C_{atm} - \delta^{13}C_{inc})} \quad (2)$$

A mass balance approach was used to determine the fractions of ancient (fOCa) and young organic carbon (fOCy) as well as of inorganic carbon (fIC) in the CO_2 flux using the $F^{14}C$ and $\delta^{13}C$ values of the potential sources (**Table 2**) and of the CO_2 released in the field and during the incubation experiment (**Supplementary Tables S2, S3**) according to **Eq. 4** and **Eq. 5**:

$$\delta^{13}C_{CO2} = f_{IC}*\delta^{13}C_{IC} + f_{OCa}*\delta^{13}C_{OCa} + f_{OCy}*\delta^{13}C_{OCy} \quad (3)$$

and

$$F^{14}C_{CO2} = f_{IC}*F^{14}C_{IC} + f_{OCa}*F^{14}C_{OCa} + f_{OCy}*F^{14}C_{OCy} \quad (4)$$

$\delta^{13}C_{CO2}$ and $F^{14}C_{CO2}$ are the mean isotopic ratios of the CO_2 released from the thaw layer at each site. In the incubations, the mean isotopic values were weighted by the CO_2 production of each depth interval per site.

Average isotopic values of IC and OC in the whole thaw layer ($F^{14}C_{IC/OC}$, $\delta^{13}C_{IC/OC}$), were calculated by weighing the respective values from the different depth intervals with their IC or OC content (IC_i/OC_i), respectively, and considering the bulk density (ρ_i) and thickness of the depth interval (h_i) according to **Eq. 5** and **Eq. 6**.

$$\overline{F^{14}C_{IC/OC}} = \sum_{i=1}^{n} F^{14}C_i \times \left(\frac{\frac{IC/OC_i}{100} \times \rho_i \times h_i}{\sum_{i=1}^{n} \frac{IC/OC_i}{100} \times \rho_i \times h_i} \right) \quad (5)$$

$$\overline{\delta^{13}C_{IC/OC}} = \sum_{i=1}^{n} \delta^{13}C_i \times \left(\frac{\frac{IC/OC_i}{100} \times \rho_i \times h_i}{\sum_{i=1}^{n} \frac{IC/OC_i}{100} \times \rho_i \times h_i} \right) \quad (6)$$

For each site, different endmembers were used for defining young ($\delta^{13}C_{OCy}$ and $F^{14}C_{OCy}$) and ancient OC ($\delta^{13}C_{OCa}$ and $F^{14}C_{OCa}$) in the mass balance approach because the sediments are composed of different materials and the sites are situated at

different heights above mean river level (a.m.r.l.) on the thaw slump (**Table 2**, **Supplementary Table S1**). The thaw mound (TM2) in the Pleistocene Yedoma is located at 30 m a.m.r.l., which is 8 m below the Holocene terrace (HT1). We defined the ancient OC and IC endmembers of TM2 as the average $\delta^{13}C$ and $F^{14}C$ content of the thaw layer weighted by its OC or IC content and bulk density. Contributions of young OC were assumed to derive mainly from the thaw layer at HT1, which had a close to modern ^{14}C content (0.984 $F^{14}C$). At the slump floor (SF3), different sediments have been mixed due to erosional processes. As for TM2, we assumed that young OC was delivered mainly from the eroded thaw layer at HT1. SF3 is located at 29 m a.m.r.l., which is lower than TM2. Thus, we chose a nearby thaw mound (TM1) that is on the same height as SF3 as ancient endmember and calculated the average $\delta^{13}C$ and $F^{14}C$ for the thaw layer as for TM2. Because the IC content of the TM1 sediment was very low, only two depth intervals could be analyzed for ^{14}C in IC and results were averaged. At HT1, IC was below the detection limit. We therefore used a two-pool mixing model considering only ancient and young OC sources contributing to respired CO_2. The $F^{14}C$ and $\delta^{13}C$ values of atmospheric CO_2 measured at this site (**Supplementary Table S2**) were used as young OC endmembers assuming that fresh plant OM contains the same isotopic ratios. The ancient OC endmember was defined by the lowest depth interval in the thaw layer at HT1.

Because of the differences in sediment ages at the three sites, the term "ancient" refers to OC and IC older than 4,000 years BP at SF3 and HT1 and Pleistocene-aged at TM1, respectively. The term "young" denotes OC younger than 4,000 years BP at TM1 and SF3, while it is near modern atmospheric ^{14}C concentrations at HT1 (**Table 2**).

To find feasible solutions for fIC, fOCa, and fOCy in **Eq. 4** and **Eq. 5**, the mass balance was solved using IsoSource (Phillips and Gregg, 2003). IsoSource iterates possible combinations of each source's contribution in pre-defined increments (1%) and within a defined tolerance (0.1‰). This underdetermined system (two equations with three variables) has no unique solution. Hence, a distribution of possible solutions is determined based on the isotopic ratios of three potential C sources (**Table 2**) that may contribute to the CO_2 emissions. By simplifying our model for HT1, fIC in **Eq. 5** and **Eq. 6** equals 0 and makes the equation system uniquely solvable.

The upper (maximum) and lower (minimum) limit of the calculated distributions of C sources were furthermore used to calculate the absolute amount of C released as CO_2 from the different C source at SF3 and TM2 after 175 and 537 days of the incubation experiment.

RESULTS

Bulk Sediment Analysis

The undisturbed Yedoma exposed as thaw mound (TM2) had the lowest ^{14}C contents in the range of 0.023–0.109 $F^{14}C_{OC}$ in the thaw layer (0–70 cm depth) corresponding to conventional ^{14}C ages of 17,830 to 29,790 years BP (**Supplementary Table S1**). The uppermost 10 cm had a higher ^{14}C content (0.109 $F^{14}C_{OC}$) than

the underlying sediment at 10–70 cm depth (0.023–0.029 $F^{14}C_{OC}$). $F^{14}C_{OC}$ values in the thaw layer of the mixed sediment on the slump floor (SF3) ranged between 0.607 $F^{14}C_{OC}$ and 0.844 $F^{14}C_{OC}$ in 0–60 cm depth (1,370–4,010 years BP) and included two younger layers at 0–10 cm and 30–50 cm depth with 0.844 $F^{14}C_{OC}$ and 0.789–0.829 $F^{14}C_{OC}$ (1,370 and 1,500–1,900 years BP), respectively. The soil developed on the Holocene terrace (HT1) had the highest ^{14}C content between 0.597 and 0.946 $F^{14}C_{OC}$ in 0–17 cm depth. The organic layer on top of the mineral soil, which was removed prior to CO_2 analysis, had a ^{14}C content slightly above atmospheric levels (1.149 $F^{14}C$) indicating the contribution of OM produced during times of higher atmospheric ^{14}C levels due to above ground nuclear weapon testing.

The $\delta^{13}C_{OC}$ results ranged from −25.3 to −32.3‰ with no clear differences between sites and no relation to sediment depth or to other parameters (**Supplementary Table S1**).

The OC and N contents did not change considerably with increasing sediment depth, except at HT1 (**Supplementary Table S1**). Here, the highest OC content was measured in the uppermost layer (9.2–9.7%) and the lowest OC content in the bottom layer (3.0%). At the mixed site (SF3), OC contents ranged from 3.9 to 5.5%, while they were considerably lower in the intact thaw mound (TM2) with values of 1.0–2.0%. Here, higher values were measured in 0–10 cm than in 10–70 cm (**Supplementary Table S1**). Similar to OC contents, the N content was highest in the uppermost layer at HT1 (0.70%) than in the lower layer (0.17%). Slightly lower N contents were determined SF3 (0.22–0.37%) and even lower values at TM2 (0.12–0.19%), which were higher in the upper 10 cm and lower below. The differences in OC and N content between the sites resulted in similar differences in OC/N ratios. HT1 had the highest values (14.0–37.6), SF3 slightly lower (13.9–17.4) and TM2 the lowest ratios (7.8–11.0).

No IC was measurable in the HT1 soil. At SF3, the IC content ranged from 1.1–2.8% in 0–50 cm, with considerably lower IC values of 0.2 and 0.7% in 20–30 cm and 50–60 cm depth, respectively. At TM2, IC contents were more consistent and ranged from 0.5–0.8%.

The ^{14}C and ^{13}C contents of the IC did not change with sediment depth. At SF3, $F^{14}C_{IC}$ values were in the range of 0.609–0.844 and thus were similar to the respective $F^{14}C_{OC}$, while the $\delta^{13}C_{IC}$ values were much higher in the range of −9.1 to −12.8‰. At TM2, $F^{14}C_{IC}$ was between 0.019 and 0.056, which is higher than the respective $F^{14}C_{OC}$, except in the uppermost interval. Here, ^{14}C contents of the IC were lower compared to values of the OM. $\delta^{13}C_{IC}$ ranged from −4.5 to −7.0‰ in the thaw mound sediment.

The pH values at HT1 (4.3–5.8) and SF3 (4.9–6.1) were slightly acidic, while they were neutral to slightly alkaline (6.4–7.8) at TM2 (**Supplementary Table S1**).

CO$_2$ Fluxes and C Isotopic Signatures

The ^{14}C content of the CO_2 respired in the field differed distinctly between sites (**Supplementary Table S2**). The CO_2 respired from TM2 had the lowest ^{14}C contents between 0.230 and 0.329 $F^{14}C$

(8.9–11.8 kyrs BP) compared to the two other sites on the thaw slump (**Supplementary Table S2**). ^{14}C concentrations of the CO_2 released from SF3 ranged between 0.547 and 0.716 $F^{14}C$ (2.7–4.9 kyrs BP), while they were close to atmospheric contents (1.022 $F^{14}C$) at HT1 with 0.975–0.985 $F^{14}C$ matching values of bulk OC in the uppermost (0–11 cm) layer (0.946 $F^{14}C$) (**Supplementary Table S1**).
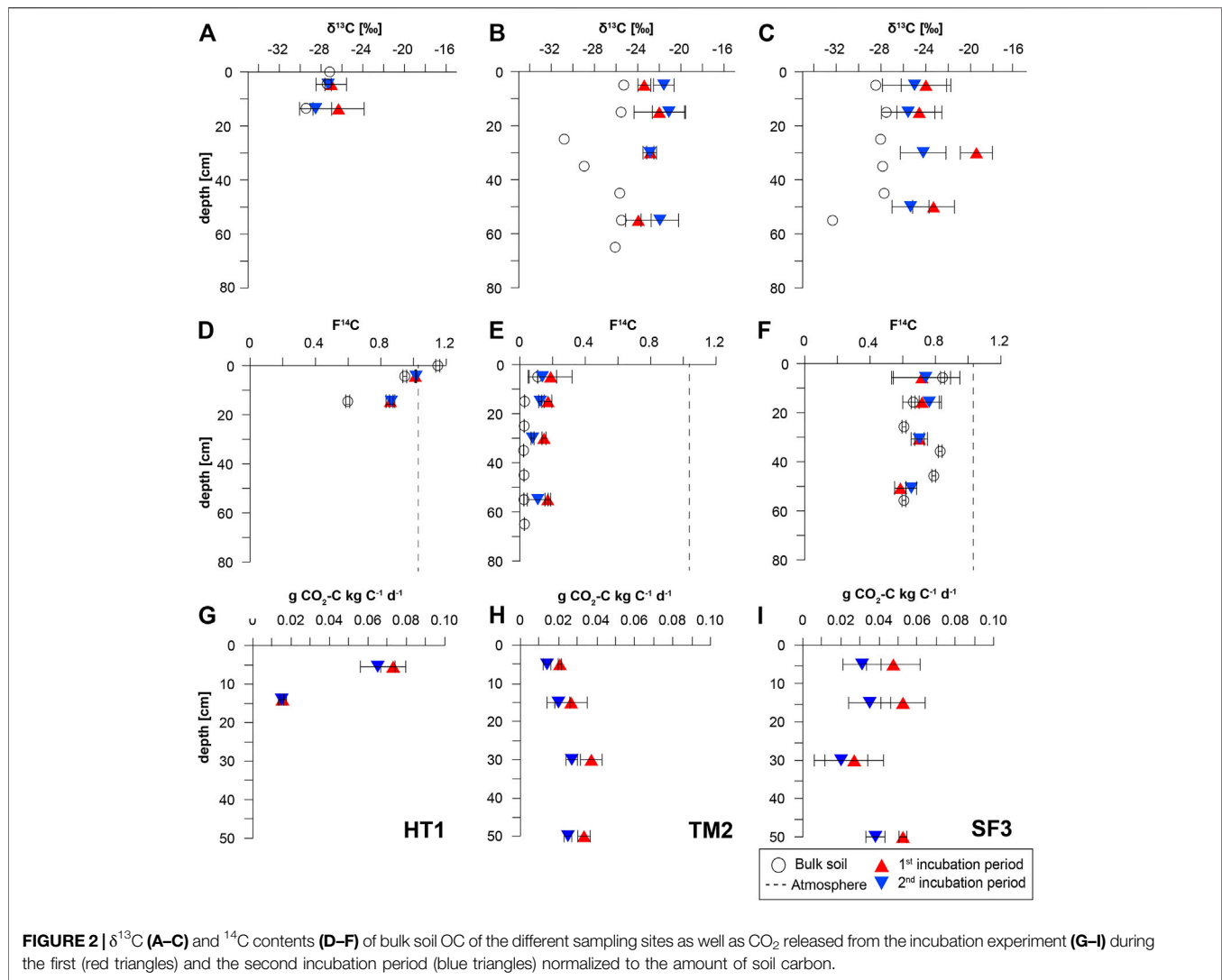
The CO_2 fluxes measured prior to CO_2 sampling for isotopic analysis varied considerable between the different sites and between the three replicates taken at each site (**Supplementary Table S2**). CO_2 fluxes were highest at TM2 (2.7–12.3 g CO_2 m^{-2} d^{-1}) and SF3 (6.1–11.6 g CO_2 m^{-2} d^{-1}) with a considerable scatter, while they were much lower at HT1 (0.8–2.0 g CO_2 m^{-2} d^{-1}). However, the results were affected by weather conditions at the day of measurements and thus difficult to compare.

The stable carbon isotopic composition of CO_2 released in the incubation experiment differed between sites and duration of the incubation (**Figure 2**, **Supplementary Table S3**). At TM2, $\delta^{13}C$ values of the CO_2 released from the different depth intervals after the first incubation period ranged between −22.0 and −23.4‰ (**Figure 2B**), which is consistently heavier than values of OC from the corresponding bulk sediment (−25.3 to −30.8‰). Even higher values were determined for the CO_2 emitted from the mixed site, SF3, in the range of −19.5 to −24.6‰ (**Figure 2C**), while OC values of the corresponding bulk sediment ranged between −27.5 and −32.3‰. In contrast, CO_2 produced from the active layer of HT1 had the lowest isotopic ratios of −27.0 and −26.3‰ in 0–11 cm and 11–17 cm depth, respectively (**Figure 2A**). No depth trend of stable isotope signatures of the CO_2 produced in the incubations could be determined at all sites.

At TM2 and SF3 $\delta^{13}C$ values decreased at the end of the incubation by 0.9–2.0‰, except for the 20–40 cm interval and ranged between −21.1 and −22.9‰ at TM2 (**Figure 2B**) and −24.2 and −25.6‰ at SF3 (**Figure 2C**). The $\delta^{13}C$ of CO_2 released from HT1 remained close to values measured after the first incubation period at −27.3 to −28.5‰ with slightly lighter values for the 11–17 cm depth interval.

The overall lowest ^{14}C contents of the CO_2 released after the first incubation period were measured at TM2 and ranged from 0.147–0.188 $F^{14}C$ (**Figure 2E**; **Supplementary Table S3**), which is higher than values of the bulk sediment (0.023–0.109 $F^{14}C$). At the mixed site, SF3, the released CO_2 had higher ^{14}C contents ranging from 0.585 to 0.718 $F^{14}C$ (**Figure 2F**) with higher values in the upper intervals 0–40 cm (0.702–0.718 $F^{14}C$) and lower values in 40–60 cm (0.585 $F^{14}C$), the latter being lower than the $F^{14}C$ of the bulk sediment. At HT1, CO_2 from the first incubation period had an overall higher ^{14}C content (**Figure 2D**) than the respective bulk sediment with 1.011 $F^{14}C$ in 0–11 cm, which is just below the atmospheric ^{14}C content measured at this site (1.021 $F^{14}C$; **Supplementary Table S2**), while 0.859 $F^{14}C$ was measured for CO_2 of the incubations from 11–17 cm depth.

The ^{14}C contents of the CO_2 changed slightly at the end of the long-term incubation (**Supplementary Table S3**). At TM2, consistently lower values were measured in all depth intervals (0.077–0.138 $F^{14}C$) after 1.5 years than after few weeks of incubation (**Figure 2E**). In contrast, ^{14}C contents increased

FIGURE 2 | δ^{13}C **(A–C)** and ^{14}C contents **(D–F)** of bulk soil OC of the different sampling sites as well as CO$_2$ released from the incubation experiment **(G–I)** during the first (red triangles) and the second incubation period (blue triangles) normalized to the amount of soil carbon.

during the incubation of SF3 sediment (0.652–0.762 F^{14}C), except for the CO$_2$ released from 20–40 cm (0.701 F^{14}C) (**Figure 2F**). The CO$_2$ produced from HT1 soil had similar values (0.864–1.016 F^{14}C) within the measurement uncertainty after few weeks and 1.5 years of incubation (**Figure 2D**).

The daily CO$_2$ production during the aerobic incubation differed considerably between sites and duration of the incubation (**Supplementary Table S3**). The lowest cumulative CO$_2$ production was measured at TM2 in the range of 0.41 and 0.76 µg CO$_2$-C gdw^{-1} d^{-1} after 175 days. Higher CO$_2$ production rates were measured for the mixed sediments from SF3 of 1.18–2.85 µg CO$_2$-C gdw^{-1} d^{-1}. At HT1, most CO$_2$ was released from the uppermost depth interval after 175 days with 7.54 µg CO$_2$-C gdw^{-1} d^{-1}, while much less CO$_2$ was produced from 11–17 cm with 0.55 µg CO$_2$-C gdw^{-1} d^{-1}, which is comparable to the rates measured in TM2 sediment. When normalized to the amount of available thawed C, the daily release of C as CO$_2$ corresponds to 0.021–0.037 g CO$_2$-C kgC^{-1} d^{-1} at TM2 (**Figure 2H**), 0.027–0.052 g CO$_2$-C kgC^{-1} d^{-1} at SF3 (**Figure 2I**), and between 0.015 and 0.093 g CO$_2$-C

kgC^{-1} d^{-1} at HT1 (**Figure 2G**, **Supplementary Table S3**). The CO$_2$ production decreased towards the end of the incubation, after 1.5 years, by about 30% both, at TM2 (0.28–0.55 µg CO$_2$-C gdw^{-1} d^{-1}) and at SF3 (0.89–1.90 µg CO$_2$-C gdw^{-1} d^{-1}), and much less, by about 8%, at HT1 (0.51–6.68 µg CO$_2$-C gdw^{-1} d^{-1}). Accordingly, the normalized C release at the end of the incubation experiment decreased to 0.014–0.027 g CO$_2$-C kgC^{-1} d^{-1} at TM2, to 0.020–0.038 g CO$_2$-C kgC^{-1} d^{-1} at SF3, and to 0.015–0.065 g CO$_2$-C kgC^{-1} d^{-1} at HT1.

Contributions of Organic and Inorganic Sources to CO$_2$ Release

A three C pool, two isotope (^{13}C, ^{14}C) mass balance approach was used to calculate the contribution of different C sources to CO$_2$ emissions in the field and during the incubation experiment for sites TM2 and SF3 (**Figure 3**). Since HT1 contained no IC, a two-pool model excluding IC was applied.

The range of possible contribution of the three different carbon sources to the CO$_2$ efflux is shown in **Table 3** and the
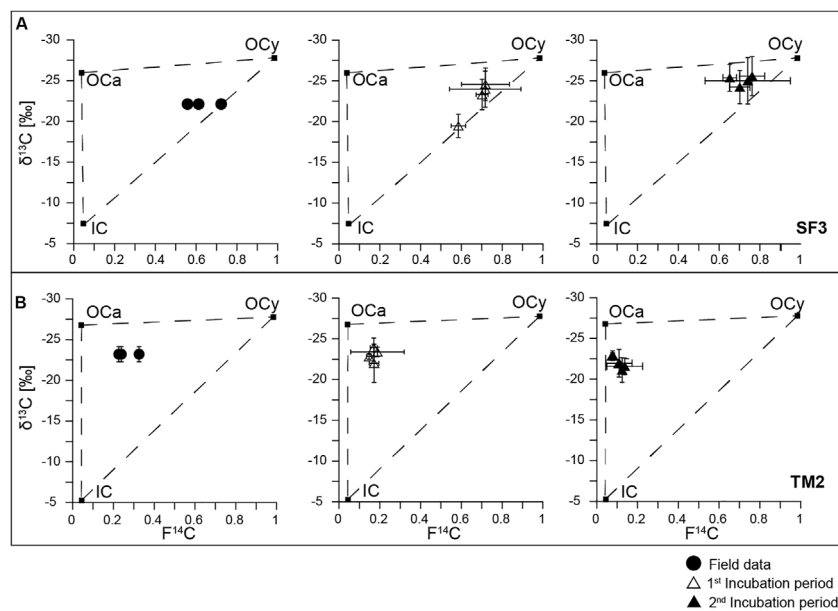
FIGURE 3 | Carbon isotope biplots for **(A)** SF3 and **(B)** TM2 indicating endmembers (squares) on which the three-pool mass balance approach is based and including field and incubation data (mean values of depth intervals and standard deviation).

TABLE 3 | Distributions of C pools contributing to the CO$_2$ released in the field and in the incubations.

Site	Minimum feasible fraction CO$_2$			Maximum feasible fraction CO$_2$		
	OCy	OCa	IC	OCy	OCa	IC
FIELD MEASUREMENTS						
TM2	0.15	0.48	0.18	0.34	0.67	0.18
SF3	0.51	0.02	0.24	0.72	0.25	0.26
HT1	0.87	0.09	-	0.91	0.13	-
1ST INCUBATION PERIOD						
TM2	0.03	0.59	0.17	0.23	0.80	0.18
SF3	0.56	0	0.24	0.74	0.20	0.26
HT1	0.94	0.04	-	0.96	0.06	-
2ND INCUBATION PERIOD						
TM2	0	0.61	0.22	0.17	0.78	0.22
SF3	0.61	0.06	0.10	0.81	0.29	0.13
HT1	0.95	0.03	-	0.97	0.05	-

corresponding absolute amount of CO$_2$ released as C in **Supplementary Table S4**. During the field measurements, most of the CO$_2$ (82%) released from the Yedoma thaw mound TM2 derived from OC sources including 15–34% of young OC and 48–67% of ancient OC. However, a significant amount of the CO$_2$ emissions of about 18% was of inorganic origin. At the mixed site SF3, a similar large amount of 74–76% of the CO$_2$ was released from organic sources. However, the majority of CO$_2$ at this site originated from young OC (51–72%) and less from ancient OC (2–25%). An even larger amount of 24–26% of the CO$_2$ derived from IC. At HT1, the two-pool model revealed that here mainly modern OM was mineralized and released as CO$_2$ (87–91%), while older

substrates from greater depth made up only 9–13% of the CO$_2$ flux.

During the first 159–189 days of the aerobic incubation, until CO$_2$ was sampled, about 82% of the CO$_2$ produced from TM2 sediment was released from OC sources including 3–12% or 15–23% young (13–14% exceeds the 0.1‰ model tolerance) and 71–80% or 59–67% ancient OC. A significant amount of 17–18% of the CO$_2$ originated from IC. At SF3, slightly less CO$_2$ of about 74–76% was released from OC during the first 41–99 days until CO$_2$ sampling. Most of this CO$_2$, between 56–74%, was of young origin, while only 0–20% derived of ancient organic sources. The remaining 24–26% of the CO$_2$ originated from IC. At HT1, modern OC was the major

CO_2 source (94–96%), while only 4–6% originated from older OM.

The largest change in C sources at the end of the incubation experiment (after 537 days) was measured at TM2. Here, the contribution of IC in the CO_2 produced increased to 22%, while the fraction of young OC decreased to 0–17% and the ancient OC contribution to 61–78%. At SF3, slightly more CO_2 was released from young (61–81%) and ancient OC (6–29%), respectively, while IC contributions decreased from 24–26% to 10–13%. No significant change in C sources during the incubation period was determined at HT1 (3–5% fOCa; 95–97% fOCy).

DISCUSSION

Carbon Sources of *in situ* CO_2 Fluxes

The analyses of CO_2 collected in the field revealed that the largest proportion of the emissions (48–67%) released from freshly thawed Yedoma (TM2) derived from the degradation of ancient OM, while a much smaller amount is mineralized from young OM (15–34%). This result agrees well with high respiration rates of Pleistocene-age Yedoma measured in previous incubation experiments (Dutta et al., 2006; Zimov et al., 2006; Lee et al., 2012) that were related to higher amounts of labile OM than in Holocene deposits (Walz et al., 2018). The young OM at TM2 most likely was deposited on top of the thaw mound by melt water and erosion. The $\delta^{13}C$ signatures of the CO_2 released in the laboratory incubations indicate that about 18% of the CO_2 released at the field sites originated from IC sources. However, we cannot rule out that the CO_2 release from carbonates during the incubations was biased by the incubation conditions. Measurements of the stable C isotope signatures of CO_2 released from the thaw slump and flux measurements would be required to construct Keeling plots (Keeling, 1958; Kohler et al., 2006) giving direct evidence for IC dissolution under *in situ* conditions. Although the IC content of the sediment was relatively low (0.5–0.8%) and the pH neutral to slightly alkaline (7.3–7.8 in 0–60 cm and 6.4 in 60–70 cm) it is possible that in this pH range, the soil or sediment pH is buffered by carbonate dissolution to bicarbonate (HCO_3^-), which is dissolved in ground water (Guo et al., 2015; Raza et al., 2020). However, for net CO_2 emissions to be produced from IC, it has been speculated that the chemical equilibrium of chemical weathering must have been shifted by organic acids towards carbonate dissolution (Zolkos et al., 2018). As suggested by Zolkos et al. (2018), thermokarst activity in retrogressive thaw slumps can increase HCO_3^- concentrations in the pore water of the sediments thus changing the chemical equilibrium to favor dissolution of carbonate and degassing of CO_2 (Fritz et al., 2015).

At the slump floor (SF3), where thermokarst processes caused the mixing of Pleistocene Yedoma with younger sediments eroded from the Holocene terrace, mostly young OM (51–72%) was released as CO_2 and much less derived from Pleistocene-age OM (2–25%). This indicates the preferential mineralization of the admixed Holocene-age OM. At SF3, thermokarst-related sediment mixing resulted in higher IC contents (0.2–2.8%) and lower pH values (4.9–6.1) promoting

IC-derived CO_2 emissions. Here, the amount of IC in the CO_2 emissions (24–26%) was even larger than in the Yedoma thaw mound (TM2) supporting observations by (Zolkos et al., 2018, 2020) that thermokarst amplifies IC cycling. The lower pH of the mixed sediment may result from higher OC and N contents that possibly supported the formation of organic acids causing the dissolution of $CaCO_3$ (Ramnarine et al., 2012; Tamir et al., 2012; Zolkos et al., 2018).

The sedimentary IC most probably is not derived from lithogenic sources because it exhibited lower $\delta^{13}C$ values (**Supplementary Table S1**) than average values for lithogenic IC in exchange with fresh water of about 2–4‰ PDB (Weber and Bergenback, 1965). Besides, the IC had similar ^{14}C concentrations like the sedimentary OC indicating coeval formation. Ca^{2+} may have been leached from silicate minerals to form pedogenic carbonate coatings on clay and silt-sized particles without lithogenic carbonates being present in the sediment (Schlesinger, 1985; Cailleau et al., 2005; Rovira and Vallejo, 2008; Ramnarine et al., 2012). Pedogenic carbonate may also have formed from HCO_3^- derived from CO_2 emitted by microbial degradation of the OM. The $\delta^{13}C$ of the pedogenic carbonate thus is lighter, in the range of −10 to 0‰ PDB, compared to lithogenic carbonate (Cerling, 1984). A further source of IC may be ostracods that lived in polygon centers during the Pleistocene and became part of the present Yedoma sediment. The $\delta^{13}C$ values of the sedimentary IC at SF3 (−9.1 to −12.8‰ PDB; **Supplementary Table S1**) agree well with reported $\delta^{13}C$ values of subfossil ostracod valves found in thermokarst lakes at Kurungnakh Island (−6.9 to −7.1‰ PDB) and subfossil intrapolygonal ostracod valves (−10.8 to −11.1‰ PDB; Wetterich et al., 2008b). Thus, a fraction of the sedimentary IC may also have derived from dissolution of these fossil remains. Further investigations are needed to disentangle potential IC sources more precisely, because the dissolution of pedogenic carbonates would release CO_2 that originally formed from microbial degradation of OM and would therefore not alter the net CO_2 emissions of the sediment from where it is released (Zolkos et al., 2018).

The Holocene terrace (HT1) was investigated because it was used as modern endmember in the isotopic mass balance calculation. At HT1 mainly modern OM with atmospheric ^{14}C content was degraded and released as CO_2 (87–91%), while the remaining fraction of the CO_2 originated from the OM stored in the deeper mineral soil intervals, as indicated by the abrupt decrease in $F^{14}C$ of the bulk soil below 17 cm depth (**Supplementary Table S1**). The soil did not contain any measurable IC. Although the vegetation was removed from HT1, small contributions of modern CO_2 derived from autotrophic respiration of roots cannot be fully excluded. However, these may be negligible, because the ^{14}C results of the CO_2, which were close to the atmospheric values, were corrected for atmospheric CO_2 contributions (**Eq. 1** and **Eq. 2**). However, if any root remains released bomb-spiked enriched $^{14}CO_2$, it would have slightly skewed our results towards modern OM.

The CO_2 produced after few weeks of the aerobic incubation represent the emissions of approximately one thaw season,

i.e., about 120 days (Boike et al., 2013). The results of the mass balance approach were similar to the field data at SF3 but slightly different at TM2 and HT1. No positive priming promoting the decomposition of the old OM as demonstrated in previous incubations (Wild et al., 2016; Walz et al., 2018; Pegoraro et al., 2019) took place at the slump floor SF3, where Holocene-age sediments were mixed with Pleistocene-age Yedoma (**Supplementary Table S4**). Most CO_2 was released from young OM (2.6–6.8 g CO_2-C kgC^{-1}) and much less from ancient OM (0–1.8 g CO_2-C kgC^{-1}) indicating the preferential mineralization of young sources. In contrast to the field data, less CO_2 was produced from young OM (3–23%; 0.1–1.5 g CO_2-C kgC^{-1}) from the Yedoma thaw mound TM2 during the first few weeks of the incubation. This suggests that less young organic substrates were present and thus were rapidly consumed, i.e., within roughly one thawing season. This result agrees well with high CO_2 production rates measured in previous aerobic incubation studies of Yedoma that were attributed to the presence of labile OM, which can be readily mineralized after thawing (Dutta et al., 2006; Lee et al., 2012; Knoblauch et al., 2013; Walz et al., 2018). At SF3 and TM2, the contribution of IC to the total CO_2 flux was similar to the field data (17–18%). The CO_2 produced during 41–159 days of incubation of soil from the Holocene terrace (HT1) contained slightly, but statistically not significant higher amounts of young OC compared to the field data. This may be related to the CO_2 collection with respiration chambers giving a mixed signal that may also include CO_2 from deeper parts of the thawed layer (21 cm) containing older OC while the CO_2 in the incubation experiment was only released from the uppermost 17 cm.

The CO_2 production from the Yedoma thaw mound at TM2 during the first 175 days of (0.41–0.76 µg CO_2-C gdw^{-1} d^{-1}) was very low compared to previous results in which Pleistocene-age Yedoma from the Kolyma region was incubated for a shorter period (41–99 days) resulting in about five times larger CO_2 production rates compared to TM2 (Dutta et al., 2006), or, up to one order of magnitude larger CO_2 production rates in an incubation at higher temperatures (15°C, Lee et al., 2012). These differences may be related to different OM composition, stage of degradation and bioavailability, i.e., interaction with mineral particles in the heterogeneous Yedoma deposits and of cause to the different incubation temperatures.

The highest CO_2 production was measured in the uppermost, youngest layer at HT1 and much less in the lower depth interval (10–17 cm; 0.55 µg CO_2-C gdw^{-1} d^{-1}). This difference is related to the larger amounts of young (close to atmospheric ^{14}C levels), little degraded substrates in the surface layer having high OC content (9.7%) and OC/N ratio (14). Likewise, more than three times higher production rates were measured for the mixed sediment at the slump floor containing more OC compared to the Yedoma thaw mound (**Supplementary Table S1**). These data underline the strong relation of CO_2 production to OC content ($R^2 = 0.9$; $p < 0.005$) persistent for all sites and both, field and incubation data, and, to a lesser extent, to OM quality represented by the OC/N ratio. The latter may have promoted the mineralization of OM, which has a lower stage of degradation

at SF3 and HT1, suggested by higher OC/N ratios compared to TM2.

The CO_2 production rates normalized to the available C differed in a smaller range between the sites (**Supplementary Table S3**). Most CO_2 was still produced from the carbon-rich surface soil at HT1, while about 40–70% less was generated from the mixed sediment SF3 (except from 20–40 cm depth) and about 25% less from the Yedoma thaw mound at SF3. The varying CO_2 production rates can be explained by the higher amount of younger OM that is preferentially degraded in HT1 soil and SF3 sediments. In addition, physical stabilization processes may reduce the bioavailability of the OM differently in the different sediments (Höfle et al., 2013; Gentsch et al., 2015).

The results measured after 1.5 years of incubations can give information on the future development of OM degradation and CO_2 production as shown in previous long-term incubation studies (Dutta et al., 2006; Knoblauch et al., 2013; Faucherre et al., 2018). The trend of young OM depletion in the thaw mound TM2, which was observed during the initial period of the incubation, continued resulting in a further decline of this OM pool by about 3–6% at the end of the incubation. Carbon dioxide emissions from ancient sources thus increased of which about 2% originate from the mineralization of Yedoma-derived OM and a larger proportion of 4–5% from the abiotic degradation of IC. Given the length of the long-term incubation, it is possible that the degradation of OM led to the oxidation of NH_4^+, which releases H^+ ions in aerated TM2 sediments during the incubation that decreased the pH and thus increased the dissolution of IC and consequently the contribution of IC to total CO_2 release (Tamir et al., 2012). The amino acids that are required for the microbial oxidation, if not present initially, may have been released into the sediment dissolved in water from melted ice wedges (Drake et al., 2015), leading to acidification of the sediment, which was experimentally shown to occur rapidly within few weeks (Tamir et al., 2011, Tamir et al., 2012).

At the mixed site SF3, slightly more CO_2 was released from both, young and old OM, while IC contribution declined at the end of the incubation. The lower contribution of IC may be caused by the overall decreasing heterotrophic respiration during the long-term incubation (**Supplementary Table S3**). The 50% lower proportion of IC may be related to the reduction of microbial respiration and CO_2 production from OM. A decreased CO_2 concentration could slow down carbonate dissolution and reduce IC emissions. In contrast to TM2, the soil of SF3 had a lower pH that indicates a lower concentration of inorganic carbon. These could have dissolved the carbonates in the sediment, which may occur as rapidly as within 1 year (Biasi et al., 2008).

The CO_2 production from the thaw layer of the sediments at TM2 and SF3 decreased at the end of the incubation by about the same amount of approximately 24–34%, while it decreased much less, by 6–11%, at HT1. This decline in CO_2 production at all sites is smaller compared to previous long-term incubations, which attributed the reduction in production rates to a decline of labile OM (Dutta et al., 2006; Knoblauch et al., 2013; Walz et al., 2018). Thus, the lower decrease in CO_2 production in this study, may indicate that less labile OM was present here.

Overall, our source assessment indicates that relative proportions of CO_2 derived from young OM in Pleistocene-age Yedoma decline during the incubation (of TM2). However, when young OM is available in sufficient amounts, like in the mixed sediment SF3 and the soil in the Holocene terrace HT1, most of the CO_2 is produced from this young OM pool during the entire duration of the incubation. The reduction in CO_2 production thus may be related to other effects, e.g., changes in the microbial community as a result of the length of the experiment, the lack of nutrients that may have led to a decreased microbial diversity and favored conditions for slower metabolizing oligotrophic bacteria, which has been proposed but not yet experimentally verified (Schädel et al., 2020).

CONCLUSION

The dual carbon isotopic source assessment revealed that large proportions of up to 80% ancient organic and about 18% inorganic carbon, despite not being shown directly in the field, were likely released from freshly thawed, Pleistocene-age Yedoma exposed as thaw mound in a retrogressive thaw slump. A young OM pool, which derived from overlaying sediments or was transported by meltwater to the thaw mound, was preferentially respired. The contribution of ancient C sources, both organic and inorganic, to the CO_2 produced from thawed Yedoma may further increase (by about 6–7%) upon longer thaw as indicated at the end of the aerobic incubation at $4°C$ after 1.5 years. The mixing of Pleistocene-age Yedoma with Holocene material at the slump floor by erosional processes did not cause a positive priming, i.e., increasing the release of ancient OC. Most of the CO_2 (51–72%) produced from the mixed sediments originated from young OM, which was available in sufficient quantities even at the end of the incubation. CO_2 production rates were positively correlated with sedimentary OC content and decreased over the course of the incubation. Considerable amounts of IC were abiotically released as CO_2 from the freshly thawed Yedoma and from the mixed sediments, which is supposed to be related to thermokarst activities and transport of HCO_3^- by meltwater from the ice wedges into the Yedoma causing dissolution of IC. Besides, pH values may be lower by the production of organic acids during microbial OM decomposition. The substantial IC contribution to CO_2 emissions from thawing Yedoma may overestimate CO_2 fluxes from organic sources. IC-related emissions may be even larger because significantly larger amounts of sedimentary IC were found in the circumarctic region compared to this study suggesting the possibility of a yet overseen source of CO_2 emissions. The dissolution of pedogenic carbonates that formed after Yedoma thaw, from bicarbonate of organic origin, would ultimately not alter the CO_2 budget, in contrast to lithogenic sources. However, the CO_2 budget might be altered if those pedogenic carbonates formed from OC over a longer time scale and were destabilized recently. Thus, further investigations are of interest and are required to determine precisely the potential sources of the sedimentary IC.

DATA AVAILABILITY STATEMENT

The datasets of this study are available in the Zenodo online repository https://doi.org/10.5281/zenodo.5644763.

AUTHOR CONTRIBUTIONS

FUNDING

ACKNOWLEDGMENTS

SUPPLEMENTARY MATERIAL

The Supplementary Material for this article can be found online at: https://www.frontiersin.org/articles/10.3389/feart.2021.737237/full#supplementary-material

REFERENCES

Biasi, C., Lind, S. E., Pekkarinen, N. M., Huttunen, J. T., Shurpali, N. J., Hyvönen, N. P., et al. (2008). Direct Experimental Evidence for the Contribution of Lime to CO2 Release from Managed Peat Soil. *Soil Biol. Biochem.* 40, 2660–2669. doi:10.1016/j.soilbio.2008.07.011

Biskaborn, B. K., Smith, S. L., Noetzli, J., Matthes, H., Vieira, G., Streletskiy, D. A., et al. (2019). Permafrost Is Warming at a Global Scale. *Nat. Commun.* 10, 1–11. doi:10.1038/s41467-018-08240-4

Boike, J., Kattenstroth, B., Abramova, K., Bornemann, N., Chetverova, A., Fedorova, I., et al. (2013). Baseline Characteristics of Climate, Permafrost and Land Cover from a New Permafrost Observatory in the Lena River Delta, Siberia (1998-2011). *Biogeosciences* 10, 2105–2128. doi:10.5194/bg-10-2105-2013

Boike, J., Wille, C., and Abnizova, A. (2008). Climatology and Summer Energy and Water Balance of Polygonal Tundra in the Lena River Delta, Siberia. *J. Geophys. Res.* 113. doi:10.1029/2007JG000540

Cailleau, G., Braissant, O., Dupraz, C., Aragno, M., and Verrecchia, E. P. (2005). Biologically Induced Accumulations of CaCO3 in Orthox Soils of Biga, Ivory Coast. *CATENA* 59, 1–17. doi:10.1016/j.catena.2004.06.002

Cerling (1984). The Stable Isotopic Composition of Modern Soil Carbonate and its Relationship to Climate. *Earth Planet. Sci. Lett.* 71, 229–240. doi:10.1016/0012-821X(84)90089-X

Costard, F., Dupeyrat, L., Séjourné, A., Bouchard, F., Fedorov, A., and Saint-Bézar, B. (2021). Retrogressive Thaw Slumps on Ice-Rich Permafrost under Degradation: Results from a Large-Scale Laboratory Simulation. *Geophys. Res. Lett.* 48. doi:10.1029/2020GL091070

Czimczik, C. I., and Welker, J. M. (2010). Radiocarbon Content of CO2 Respired from High Arctic Tundra in Northwest Greenland. *Arctic, Antarctic, Alpine Res.* 42, 342–350. doi:10.1657/1938-4246-42.3.342

Czudek, T., and Demek, J. (1970). Thermokarst in Siberia and its Influence on the Development of Lowland Relief. *Quat. Res.* 1, 103–120. doi:10.1016/0033-5894(70)90013-X

Dewald, A., Heinze, S., Jolie, J., Zilges, A., Dunai, T., Rethemeyer, J., et al. (2013). CologneAMS, a Dedicated center for Accelerator Mass Spectrometry in Germany. *Nucl. Instr. Methods Phys. Res. Section B: Beam Interactions Mater. Atoms* 294, 18–23. doi:10.1016/j.nimb.2012.04.030

Dorsett, A., Cherrier, J., Martin, J. B., and Cable, J. E. (2011). Assessing Hydrologic and Biogeochemical Controls on Pore-Water Dissolved Inorganic Carbon Cycling in a Subterranean Estuary: A 14C and 13C Mass Balance Approach. *Mar. Chem.* 127, 76–89. doi:10.1016/j.marchem.2011.07.007

Drake, T. W., Wickland, K. P., Spencer, R. G. M., McKnight, D. M., and Striegl, R. G. (2015). Ancient Low-Molecular-Weight Organic Acids in Permafrost Fuel Rapid Carbon Dioxide Production upon Thaw. *Proc. Natl. Acad. Sci. USA* 112, 13946–13951. doi:10.1073/pnas.1511705112

Dutta, K., Schuur, E. A. G., Neff, J. C., and Zimov, S. A. (2006). Potential Carbon Release from Permafrost Soils of Northeastern Siberia. *Glob. Change Biol.* 12, 2336–2351. doi:10.1111/j.1365-2486.2006.01259.x

Estop-Aragonés, C., Cooper, M. D. A., Fisher, J. P., Thierry, A., Garnett, M. H., Charman, D. J., et al. (2018). Limited Release of Previously-Frozen C and Increased New Peat Formation after Thaw in Permafrost Peatlands. *Soil Biol. Biochem.* 118, 115–129. doi:10.1016/j.soilbio.2017.12.010

Faucherre, S., Jørgensen, C. J., Blok, D., Weiss, N., Siewert, M. B., Bang-Andreasen, T., et al. (2018). Short and Long-Term Controls on Active Layer and Permafrost Carbon Turnover across the Arctic. *J. Geophys. Res. Biogeosci.* 123, 372–390. doi:10.1002/2017JG004069

Fritz, M., Opel, T., Tanski, G., Herzschuh, U., Meyer, H., Eulenburg, A., et al. (2015). Dissolved Organic Carbon (DOC) in Arctic Ground Ice. *The Cryosphere* 9, 737–752. doi:10.5194/tc-9-737-2015

Gentsch, N., Mikutta, R., Shibistova, O., Wild, B., Schnecker, J., Richter, A., et al. (2015). Properties and Bioavailability of Particulate and mineral-associated Organic Matter in Arctic Permafrost Soils, Lower Kolyma Region, Russia. *Eur. J. Soil Sci.* 66, 722–734. doi:10.1111/ejss.12269

Griffith, D. R., McNichol, A. P., Xu, L., McLaughlin, F. A., Macdonald, R. W., Brown, K. A., et al. (2012). Carbon Dynamics in the Western Arctic Ocean: Insights from Full-Depth Carbon Isotope Profiles of DIC, DOC, and POC. *Biogeosciences* 9, 1217–1224. doi:10.5194/bg-9-1217-2012

Grigoriev, M. N. (1993). Cryomorphogenesis of the Lena River Mouth Area. *Siberian Branch, USSR Academy of Sciences, Yakutsk*, 176, 1993 (in Russian).

Grosse, G., Harden, J., Turetsky, M., McGuire, A. D., Camill, P., Tarnocai, C., et al. (2011). Vulnerability of High-Latitude Soil Organic Carbon in North America to Disturbance. *J. Geophys. Res.* 116. doi:10.1029/2010JG001507

Guo, J., Wang, F., Vogt, R. D., Zhang, Y., and Liu, C.-Q. (2015). Anthropogenically Enhanced Chemical Weathering and Carbon Evasion in the Yangtze Basin. *Sci. Rep.* 5, 1–8. doi:10.1038/srep11941

Hicks Pries, C. E., Schuur, E. A. G., Natali, S. M., and Crummer, K. G. (2016). Old Soil Carbon Losses Increase with Ecosystem Respiration in Experimentally Thawed Tundra. *Nat. Clim Change* 6, 214–218. doi:10.1038/nclimate2830

Höfle, S., Rethemeyer, J., Mueller, C. W., and John, S. (2013). Organic Matter Composition and Stabilization in a Polygonal Tundra Soil of the Lena Delta. *Biogeosciences* 10, 3145–3158. doi:10.5194/bg-10-3145-2013

Jongejans, L. L., Liebner, S., Knoblauch, C., Mangelsdorf, K., Ulrich, M., Grosse, G., et al. (2021). Greenhouse Gas Production and Lipid Biomarker Distribution in Yedoma and Alas Thermokarst lake Sediments in Eastern Siberia. *Glob. Change Biol.* 27, 2822–2839. doi:10.1111/gcb.15566

Jongejans, L. L., Strauss, J., Lenz, J., Peterse, F., Mangelsdorf, K., Fuchs, M., et al. (2018). Organic Matter Characteristics in Yedoma and Thermokarst Deposits on Baldwin Peninsula, West Alaska. *Biogeosciences* 15, 6033–6048. doi:10.5194/bg-15-6033-2018

Keeling, C. D. (1958). The Concentration and Isotopic Abundances of Atmospheric Carbon Dioxide in Rural Areas. *Geochimica et Cosmochimica Acta* 13, 322–334. doi:10.1016/0016-7037(58)90033-4

Knoblauch, C., Beer, C., Sosnin, A., Wagner, D., and Pfeiffer, E.-M. (2013). Predicting Long-Term Carbon Mineralization and Trace Gas Production from Thawing Permafrost of Northeast Siberia. *Glob. Change Biol.* 19, 1160–1172. doi:10.1111/gcb.12116

Kohler, P., Fischer, H., Schmitt, J., and Munhoven, G. (2006). On the Application and Interpretation of Keeling Plots in Paleo Climate Research – Deciphering δ¹³C of Atmospheric CO₂ Measured in Ice Cores. 18.

Kuhry, P., Bárta, J., Blok, D., Elberling, B., Faucherre, S., Hugelius, G., et al. (2020). Lability Classification of Soil Organic Matter in the Northern Permafrost Region. *Biogeosciences* 17, 361–379. doi:10.5194/bg-17-361-2020

Lantuit, H., and Pollard, W. H. (2008). Fifty Years of Coastal Erosion and Retrogressive Thaw Slump Activity on Herschel Island, Southern Beaufort Sea, Yukon Territory, Canada. *Geomorphology* 95, 84–102. doi:10.1016/j.geomorph.2006.07.040

Lee, H., Schuur, E. A. G., Inglett, K. S., Lavoie, M., and Chanton, J. P. (2012). The Rate of Permafrost Carbon Release under Aerobic and Anaerobic Conditions and its Potential Effects on Climate. *Glob. Change Biol.* 18, 515–527. doi:10.1111/j.1365-2486.2011.02519.x

Nitzbon, J., Westermann, S., Langer, M., Martin, L. C. P., Strauss, J., Laboor, S., et al. (2020). Fast Response of Cold Ice-Rich Permafrost in Northeast Siberia to a Warming Climate. *Nat. Commun.* 11, 1–11. doi:10.1038/s41467-020-15725-8

Pegoraro, E., Mauritz, M., Bracho, R., Ebert, C., Dijkstra, P., Hungate, B. A., et al. (2019). Glucose Addition Increases the Magnitude and Decreases the Age of Soil Respired Carbon in a Long-Term Permafrost Incubation Study. *Soil Biol. Biochem.* 129, 201–211. doi:10.1016/j.soilbio.2018.10.009

Phillips, D. L., and Gregg, J. W. (2003). Source Partitioning Using Stable Isotopes: Coping with Too many Sources. *Oecologia* 136, 261–269. doi:10.1007/s00442-003-1218-3

Ramnarine, R., Wagner-Riddle, C., Dunfield, K. E., and Voroney, R. P. (2012). Contributions of Carbonates to Soil CO2 Emissions. *Can. J. Soil Sci.* 92, 599–607. doi:10.4141/cjss2011-025

Raza, S., Miao, N., Wang, P., Ju, X., Chen, Z., Zhou, J., et al. (2020). Dramatic Loss of Inorganic Carbon by Nitrogen-induced Soil Acidification in Chinese Croplands. *Glob. Change Biol.* 26, 3738–3751. doi:10.1111/gcb.15101

Reimer, P. J., Bard, E., Bayliss, A., Beck, J. W., Blackwell, P. G., Ramsey, C. B., et al. (2013). IntCal13 and Marine13 Radiocarbon Age Calibration Curves 0-50,000 Years Cal BP. *Radiocarbon* 55, 1869–1887. doi:10.2458/azu_js_rc.55.16947

Rethemeyer, J., Gierga, M., Heinze, S., Stolz, A., Wotte, A., Wischhöfer, P., et al. (2019). Current Sample Preparation and Analytical Capabilities of the Radiocarbon Laboratory at CologneAMS. *Radiocarbon* 61, 1449–1460. doi:10.1017/rdc.2019.16

Routh, J., Hugelius, G., Kuhry, P., Filley, T., Tillman, P. K., Becher, M., et al. (2014). Multi-proxy Study of Soil Organic Matter Dynamics in Permafrost Peat Deposits Reveal Vulnerability to Climate Change in the European Russian Arctic. *Chem. Geology.* 368, 104–117. doi:10.1016/j.chemgeo.2013.12.022

Rovira, P., and Vallejo, V. R. (2008). Changes in δ13C Composition of Soil Carbonates Driven by Organic Matter Decomposition in a Mediterranean Climate: A Field Incubation experiment. *Geoderma* 144, 517–534. doi:10.1016/j.geoderma.2008.01.006

Schädel, C., Bader, M. K.-F., Schuur, E. A. G., Biasi, C., Bracho, R., Čapek, P., et al. (2016). Potential Carbon Emissions Dominated by Carbon Dioxide from Thawed Permafrost Soils. *Nat. Clim Change* 6, 950–953. doi:10.1038/nclimate3054

Schädel, C., Beem-Miller, J., Aziz Rad, M., Crow, S. E., and Hicks Pries, C. E. (2020). Decomposability of Soil Organic Matter over Time: the Soil Incubation Database (SIDb, Version 1.0) and Guidance for Incubation Procedures. *Earth Syst. Sci. Data* 12, 1511–1524. doi:10.5194/essd-12-1511-2020

Schädel, C., Schuur, E. A. G., Bracho, R., Elberling, B., Knoblauch, C., Lee, H., et al. (2014). Circumpolar Assessment of Permafrost C Quality and its Vulnerability over Time Using Long-Term Incubation Data. *Glob. Change Biol.* 20, 641–652. doi:10.1111/gcb.12417

Schirrmeister, L., Kunitsky, V., Grosse, G., Wetterich, S., Meyer, H., Schwamborn, G., et al. (2011). Sedimentary Characteristics and Origin of the Late Pleistocene Ice Complex on north-east Siberian Arctic Coastal Lowlands and Islands - A Review. *Quat. Int.* 241, 3–25. doi:10.1016/j.quaint.2010.04.004

Schlesinger, W. H. (1985). The Formation of Caliche in Soils of the Mojave Desert, California. *Geochimica et Cosmochimica Acta* 49, 57–66. doi:10.1016/0016-7037(85)90191-7

Schuur, E. a. G., McGuire, A. D., Schädel, C., Grosse, G., Harden, J. W., Hayes, D. J., et al. (2015). Climate Change and the Permafrost Carbon Feedback. *Nature* 520, 171–179. doi:10.1038/nature14338

Schuur, E. A. G., and Trumbore, S. E. (2006). Partitioning Sources of Soil Respiration in Boreal Black spruce forest Using Radiocarbon. *Glob. Change Biol.* 12, 165–176. doi:10.1111/j.1365-2486.2005.01066.x

Schwamborn, G., Rachold, V., and Grigoriev, M. N. (2002). Late Quaternary Sedimentation History of the Lena Delta. *Quat. Int.* 89, 119–134. doi:10.1016/S1040-6182(01)00084-2

Stapel, J. G., Schirrmeister, L., Overduin, P. P., Wetterich, S., Strauss, J., Horsfield, B., et al. (2016). Microbial Lipid Signatures and Substrate Potential of Organic Matter in Permafrost Deposits: Implications for Future Greenhouse Gas Production. *J. Geophys. Res. Biogeosci.* 121, 2652–2666. doi:10.1002/2016JG003483

Stapel, J. G., Schwamborn, G., Schirrmeister, L., Horsfield, B., and Mangelsdorf, K. (2018). Substrate Potential of Last Interglacial to Holocene Permafrost Organic Matter for Future Microbial Greenhouse Gas Production. *Biogeosciences* 15, 1969–1985. doi:10.5194/bg-15-1969-2018

Stolz, A., Dewald, A., Altenkirch, R., Herb, S., Heinze, S., Schiffer, M., et al. (2017). Radiocarbon Measurements of Small Gaseous Samples at CologneAMS. *Nucl. Instr. Methods Phys. Res. Section B: Beam Interactions Mater. Atoms* 406, 283–286. doi:10.1016/j.nimb.2017.03.031

Strauss, J., Schirrmeister, L., Grosse, G., Fortier, D., Hugelius, G., Knoblauch, C., et al. (2017). Deep Yedoma Permafrost: A Synthesis of Depositional Characteristics and Carbon Vulnerability. *Earth-Science Rev.* 172, 75–86. doi:10.1016/j.earscirev.2017.07.007

Strauss, J., Schirrmeister, L., Mangelsdorf, K., Eichhorn, L., Wetterich, S., and Herzschuh, U. (2015). Organic-matter Quality of Deep Permafrost Carbon - a Study from Arctic Siberia. *Biogeosciences* 12, 2227–2245. doi:10.5194/bg-12-2227-2015

Stuiver, M., and Polach, H. A. (1977). Discussion Reporting of 14C Data. *Radiocarbon* 19, 355–363. doi:10.1017/s0033822200003672

Tamir, G., Shenker, M., Heller, H., Bloom, P. R., Fine, P., and Bar-Tal, A. (2011). Can Soil Carbonate Dissolution Lead to Overestimation of Soil Respiration? *Soil Sci. Soc. America J.* 75, 1414–1422. doi:10.2136/sssaj2010.0396

Tamir, G., Shenker, M., Heller, H., Bloom, P. R., Fine, P., and Bar-Tal, A. (2012). Dissolution and Re-crystallization Processes of Active Calcium Carbonate in Soil Developed on Tufa. *Soil Sci. Soc. America J.* 76, 1606–1613. doi:10.2136/sssaj2012.0041

Tanski, G., Lantuit, H., Ruttor, S., Knoblauch, C., Radosavljevic, B., Strauss, J., et al. (2017). Transformation of Terrestrial Organic Matter along Thermokarst-Affected Permafrost Coasts in the Arctic. *Sci. Total Environ.* 581-582, 434–447. doi:10.1016/j.scitotenv.2016.12.152

Turetsky, M. R., Abbott, B. W., Jones, M. C., Anthony, K. W., Olefeldt, D., Schuur, E. A. G., et al. (2020). Carbon Release through Abrupt Permafrost Thaw. *Nat. Geosci.* 13, 138–143. doi:10.1038/s41561-019-0526-0

Wacker, L., Němec, M., and Bourquin, J. (2010). A Revolutionary Graphitisation System: Fully Automated, Compact and Simple. *Nucl. Instr. Methods Phys. Res. Section B: Beam Interactions Mater. Atoms* 268, 931–934. doi:10.1016/j.nimb.2009.10.067

Walz, J., Knoblauch, C., Tigges, R., Opel, T., Schirrmeister, L., and Pfeiffer, E.-M. (2018). Greenhouse Gas Production in Degrading Ice-Rich Permafrost Deposits in Northeastern Siberia. *Biogeosciences* 15, 5423–5436. doi:10.5194/bg-15-5423-2018

Weber, J. N., and Bergenback, R. E. (1965). Reconstruction of Depositional Environments in the Pennsylvanian Vanport basin by Carbon Isotope Ratios. *Sepm Jsr* Vol. 35, 36–48. doi:10.1306/74D711EA-2B21-11D7-8648000102C1865D

Weiss, N., Blok, D., Elberling, B., Hugelius, G., Jørgensen, C. J., Siewert, M. B., et al. (2016). Thermokarst Dynamics and Soil Organic Matter Characteristics Controlling Initial Carbon Release from Permafrost Soils in the Siberian Yedoma Region. *Sediment. Geology.* 340, 38–48. doi:10.1016/j.sedgeo.2015.12.004

Wetterich, S., Kuzmina, S., Andreev, A. A., Kienast, F., Meyer, H., Schirrmeister, L., et al. (2008a). Palaeoenvironmental Dynamics Inferred from Late Quaternary Permafrost Deposits on Kurungnakh Island, Lena Delta, Northeast Siberia, Russia. *Quat. Sci. Rev.* 27, 1523–1540. doi:10.1016/j.quascirev.2008.04.007

Wetterich, S., Schirrmeister, L., Meyer, H., Viehberg, F. A., and Mackensen, A. (2008b). Arctic Freshwater Ostracods from Modern Periglacial Environments in the Lena River Delta (Siberian Arctic, Russia): Geochemical Applications for Palaeoenvironmental Reconstructions. *J. Paleolimnol.* 39, 427–449. doi:10.1007/s10933-007-9122-1

Wild, B., Gentsch, N., Čapek, P., Diáková, K., Alves, R. J. E., Bárta, J., et al. (2016). Plant-derived Compounds Stimulate the Decomposition of Organic Matter in Arctic Permafrost Soils. *Sci. Rep.* 6, 25607. doi:10.1038/srep25607

Windirsch, T., Grosse, G., Ulrich, M., Schirrmeister, L., Fedorov, A. N., Konstantinov, P. Y., et al. (2020). Organic Carbon Characteristics in Ice-Rich Permafrost in Alas and Yedoma Deposits, central Yakutia, Siberia. *Biogeosciences* 17, 3797–3814. doi:10.5194/bg-17-3797-2020

Wotte, A., Wischhöfer, P., Wacker, L., and Rethemeyer, J. (2017). 14 CO 2 Analysis of Soil Gas: Evaluation of Sample Size Limits and Sampling Devices. *Nucl. Instr. Methods Phys. Res. Section B: Beam Interactions Mater. Atoms* 413, 51–56. doi:10.1016/j.nimb.2017.10.009

Zimov, S. A., Davydov, S. P., Zimova, G. M., Davydova, A. I., Schuur, E. A. G., Dutta, K., et al. (2006). Permafrost Carbon: Stock and Decomposability of a Globally Significant Carbon Pool. *Geophys. Res. Lett.* 33, L20502. doi:10.1029/2006GL027484

Zolkos, S., Tank, S. E., and Kokelj, S. V. (2018). Mineral Weathering and the Permafrost Carbon-Climate Feedback. *Geophys. Res. Lett.* 45, 9623–9632. doi:10.1029/2018GL078748

Zolkos, S., Tank, S. E., Striegl, R. G., Kokelj, S. V., Kokoszka, J., Estop-Aragonés, C., et al. (2020). Thermokarst Amplifies Fluvial Inorganic Carbon Cycling and export across Watershed Scales on the Peel Plateau, Canada. *Biogeosciences* 17, 5163–5182. doi:10.5194/bg-17-5163-2020